Fast Heavy-Ion-Induced Anion–Molecule Reactions on the Methanol Droplet Surface

Takuya Majima,[1] Yuki Mizunami,[1] Takahiro Teramoto,[2] Hidetsugu Tsuchida,[1,3] and Manabu Saito[1,3]*

1 Department of Nuclear Engineering, Kyoto University, Kyoto 615-8540, Japan

2 Institute for Radiation Sciences, Osaka University, 1-1 Machikaneyama, Toyonaka, Osaka 560-0043, Japan

3 Quantum Science and Engineering Center, Kyoto University, Uji 611-0011, Japan

ABSTRACT

To gain insight into complex ion–molecule reactions induced by MeV-energy heavy ion irradiation of condensed matter, we performed a mass spectrometric study of secondary ions emitted from methanol microdroplet surfaces by 2.0-MeV C^{2+}. We observed positive and negative secondary ions, including fragments, clusters, and reaction products. We found that a wider variety of negative ions than positive ions (such as C_2H^-, C_2HO^-, $C_2H_5O^-$, and $C_2H_3O_2^-$) were formed. We performed measurements for deuterated methanol (CH_3OD) droplets to identify the hydrogen elimination site of the intermediates involved in the reactions, and to reveal the mechanism that generates various negative reaction product ions. Comparing the

results of CH_3OD with CH_3OH droplets, we propose that the primary formation mechanism is association reactions of anion and neutral fragments, such as $CH_3O^- + CO \rightarrow C_2H_3O_2^-$. Quantum chemical calculations confirmed that the reactions can proceed with no barrier. This study provides new insight into the importance of rapid anion–molecule reactions among fragments as the mechanism that generates complex molecular species in fast heavy-ion-induced reactions.

1. INTRODUCTION

Interactions between swift heavy ions and condensed matter are of scientific interest in various fields. For example, living cells are irradiated with fast ion beams for cancer therapy.[1] In astronomical environments, cosmic rays are incident on solid-phase molecules under low-temperature conditions.[2–6] Reactions caused by cosmic rays in ice that contains organic molecules such as methanol might form prebiotic species in outer space.[3,4,7,8]

MeV-energy heavy ions deposit a large amount of energy into molecules along their trajectories via ionization and electronic excitation. As a result, various fragment ions and radicals can be produced at high density. Complex molecules are expected to be produced in secondary reactions among the fragments. Ionic products play an essential role in a series of reactions. However, the ionic species and their reactions are poorly understood because of the difficulty of analyzing and predicting complex and transient species.

Methanol, which is the simplest alcohol, is a fundamental molecule for understanding radiation-induced reactions.[9–15] Ionic products have been studied by mass spectrometry with gas phase targets since the initial days of radiation chemistry research. For example, the fragment ions obtained from gas-phase methanol after 50-eV electron impacts are CH_2OH^+ and CHO^+, produced by H and additional H_2 emissions from parent ions CH_3OH^+.[9] Subsequent ion–

molecule reactions of the fragment ions with other CH_3OH molecules were observed in high-pressure gas-phase targets, leading to production of protonated methanol ions $CH_3OH_2^+$ initiated by H^+ or H^- transfer, as follows:[10]

$$CH_3OH^+ + CH_3OH \rightarrow CH_3OH_2^+ + CH_2OH \text{ (or } CH_3O) \quad (1)$$

$$CH_2OH^+ + CH_3OH \rightarrow CH_3OH_2^+ + HCHO \quad (2)$$

$$CHO^+ + CH_3OH \rightarrow CH_3OH_2^+ + CO \quad (3)$$

$$\rightarrow CH_2OH^+ + HCHO \quad (4)$$

$$\rightarrow CH_3^+ + CO + H_2O \quad (5)$$

$$CH_3^+ + CH_3OH \rightarrow CH_2OH^+ + CH_4 \quad (6)$$

Similar reactions are also considered to proceed in condensed matter.[11] In fast heavy ion collisions, increased production of smaller fragment ions is expected because of multiple ionization,[16] although measurements of fast heavy ion collisions with isolated methanol molecules have not yet been reported, except for a highly charged projectile of 1.2-MeV Ar^{8+}.[17]

As negative fragment ions, H^-, O^-, OH^-, and CH_3O^- have been observed after dissociative electron attachment (DEA) to gas-phase methanol.[18,19] In addition to these fragments, CH_i^- (i = 0–2) and CHO^- have been observed in electron-induced fragmentation at the collision energy of 70 eV.[20,21] CH_3^- has also been reported in secondary ions emitted from a methanol ice surface by low-energy electrons.[8] In condensed matter, CH_3O^- can be produced as the result of the decay of solvated electrons by interaction with parent molecules or neutral radicals.[11,13]. However, further knowledge about negative ions (also termed anions hereafter) in condensed matter is limited.

Another mass spectrometric study of fast heavy-ion-induced reactions of methanol was performed for secondary ions emitted from ice surfaces from an astrochemical viewpoint.[3] Andrade et al. observed positive secondary ions after the impact of ^{252}Cf fission fragments (~65-

MeV heavy ions).[3] The most abundant ion was protonated methanol ions $CH_3OH_2^+$. In addition, they observed fragments H_i^+ (i = 1–3), CH_i^+ (i = 0–3), and CH_iO^+ (i = 0–3); reaction products $C_2H_i^+$ (i = 0–3); and cluster ions $(CH_3OH)_nH^+$ and $(CH_3OH)_nCHO^+$. Andrade et al. noted that swift heavy ions generate a higher variety of positive ions at 3 to 4 orders of magnitude higher probabilities than X-ray irradiation.[22] Almeida et al. reported that MeV-energy heavy ions emit secondary ions at 5 to 6 orders of magnitude higher probabilities than those by electron impact at 850- to 2200-eV.[6] To our knowledge, negative secondary ions from a methanol ice surface by fast heavy ion irradiation have not yet been reported.

In experiments using ice targets, particular care is required to avoid impurities of absorbed residual gas and reactions that pertain to the accumulated products on the ice surface when considering the elementary reaction processes. Recently, we developed an alternative experimental system that enables a mass spectrometric study of secondary ions emitted from microdroplet surfaces by fast ion impacts under high vacuum.[23,24] This method eliminates the aforementioned problems because the product ions always originate from the new fresh surface of the droplets. Furthermore, the secondary ions are considered to be emitted on a sub-nanosecond time scale.[25] Thus, they are expected to provide information on the reaction intermediates generated on this time scale. More recently, we developed a coincidence technique with forward-scattered projectiles.[26] This measurement excludes a huge number of background ions that originate from residual gas and selectively identifies the secondary ions emitted from droplet surfaces. This coincidence technique was demonstrated using ethanol droplets with 4.0-MeV C^{3+}. Although this technique highlighted the production of various reaction product ions, these ions were too complex to investigate the reaction mechanism further.

In this study, to investigate the formation processes of reaction product ions in more detail, we applied this aforementioned coincidence technique to droplets of methanol (CH_3OH), which has a simpler structure and a limited number of reaction species than ethanol. We observed positive and negative secondary ions emitted from methanol droplets by 2.0-MeV C^{2+} irradiation. In addition, we performed measurements for methanol-d (CH_3OD) droplets. By comparing the results of CH_3OH and CH_3OD droplets, we examined the formation processes of the reaction product anions with the aid of quantum chemical calculations.

2. METHODS

2.1 Experimental methods

Our experimental setup has been reported previously in detail.[24,26] Briefly, microdroplets of methanol were generated by ultrasonic atomization from liquid methanol CH_3OH (99.8% purity, Nacalai Tesque, Inc., Japan) and methanol-d CH_3OD (99.0 atom% D, Acros Organics, Belgium) samples. The diameter of the droplets in a collision area was mainly from several hundred nanometers to a few micrometers. The droplets were transported to the collision area with argon (Ar) carrier gas by using a differential pumping system. The droplet temperature was estimated to be 190–210 K.[27] The flow rate of the Ar gas was maintained at 0.3 standard liters per minute with a mass flow controller. During the measurement, the vacuum pressure in the collision chamber was ca. 2×10^{-4} Pa.

The droplets were irradiated with 2.0-MeV C^{2+} extracted from a 2-MV tandem-type Pelletron accelerator at the Quantum Science and Engineering Center, Kyoto University. The beam was collimated to 2 mm (vertical) × 1 mm (horizontal). Secondary ions produced by the collisions of the projectiles were analyzed by time-of-flight (TOF) mass spectrometry. The positive and

negative secondary ions were measured separately by reversing the polarity of the electric field. In addition, the forward-scattered projectiles at ca. 14 mrad were detected with a passivated implanted planar silicon semiconductor detector (SSD, Canberra PD50-12-100, USA) after penetrating droplets. The SSD signal was used as the start trigger of the TOF measurements. The TOF timing and SSD pulse height were recorded event-by-event in list mode. The correlation between the secondary ions and the energy of the forward-scattered particles after the measurements can thus be examined. The background ions generated from the gas-phase molecules were eliminated by selecting the appropriate energy range of the forward-scattered particles. The secondary ion yields emitted per ion impact were evaluated by dividing the integrated counts of the TOF peaks by the number of valid start triggers, and a detection efficiency of 0.42.[26]

2.2 Computational method

We performed quantum chemical calculations with the Gaussian16 package[28] in the CISD method with the aug-cc-pVDZ basis set to confirm the energetics of anion–molecule reactions proposed from the experimental results. The total energies of the reactants and possible structural isomers of product anions were compared after geometrical optimization. For $C_2H_3O_2^-$, transition states between these isomers were also investigated. In addition, we obtained potential energy curves as functions of the intermolecular distances between the reactants to evaluate the energetic feasibility of the proposed anion–molecule reactions. The calculations started from distances larger than 4 Å. The optimized structure was used as the input for the next geometrical optimization at a shorter distance. Changes in the stable structures and the total energies were traced by repeating this calculation while decreasing the intermolecular distances. Ideally, the

reaction dynamics should be studied by using multidimensional potential surfaces. The present calculations correspond to simplified evaluations by projecting the trajectories on the potential surfaces to the one-dimensional potential curves as functions of the intermolecular distances.

3. RESULTS AND DISCUSSION

3.1 Positive ions

Figure 1 shows the mass spectrum of the positive secondary ions from CH_3OH droplets. The vertical axis represents the ion counts divided by the number of start triggers, which provides the relative secondary ion yield per single incident ion. The horizontal axis is the mass-to-charge ratio (m/z) of the ions. Table 1 shows assignments of the peaks and their secondary ion yields. For comparison, Figure 2 shows a TOF mass spectrum of the product ions from gas-phase methanol molecules, obtained in a separate experiment of 4-MeV C^{3+} collisions (unpublished results). This result indicates that positive ions emitted from the droplet surface are predominantly generated by protonation, instead of direct ionization as in the gas phase.

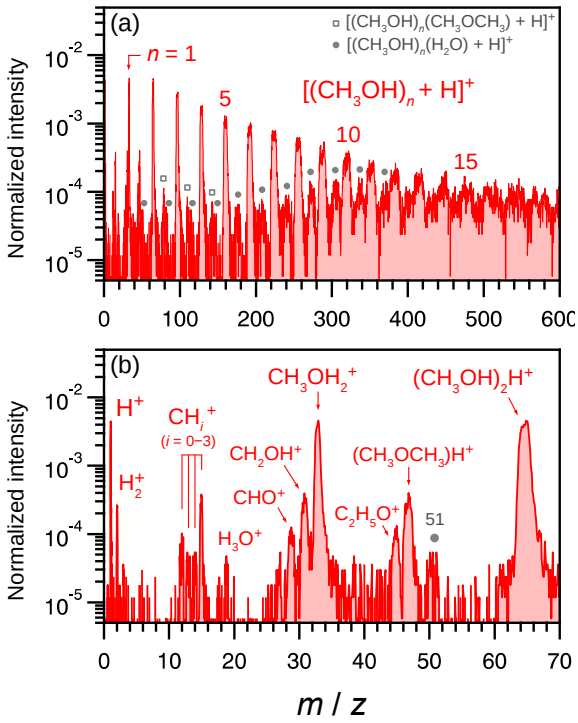

Figure 1. (a) Mass spectrum of the positive ions from CH_3OH droplets induced by 2.0-MeV C^{2+}. The vertical axis represents the counts divided by the number of start triggers. (b) Expanded mass spectrum in the range of m/z <70.

Table 1. Positive secondary ion yields emitted from CH_3OH droplets per single 2.0-MeV C^{2+} impact.[a]

m/*z*	CH_3OH droplets	
	Positive ions	Ion yields per impact ($\times 10^{-2}$)
1	H^+	5.69
2	H_2^+	0.40
12	C^+	0.16
13	CH^+	0.11
14	CH_2^+	0.10

15	CH_3^+	0.60
19	H_3O^+	0.07
29	CHO^+	0.33
31	CH_2OH^+	0.96
33	$CH_3OH_2^+$	10.08
45	$C_2H_5O^+$	0.30
47	$C_2H_7O^+$	0.97
50	$[(CH_3OH)(H_2O)]^+$	0.09
51	$[(CH_3OH)(H_2O)+H]^+$	0.04
	$([(CH_3OH)_n + H]^+)$	
65	$n = 2$	15.24
97	$n = 3$	12.86
129	$n = 4$	9.32
161	$n = 5$	7.35
193	$n = 6$	6.12
225	$n = 7$	5.71
257	$n = 8$	4.46
289	$n = 9$	3.55
321	$n = 10$	3.00
353	$n = 11$	2.35
385	$n = 12$	1.94
417	$n = 13$	1.54
	Total	93.3

[a] We did not evaluate the values for the mixed clusters because of the large uncertainties.

3.1.1 Positive cluster ions

Major product ions were protonated cluster ions $[(CH_3OH)_n + H]^+$ (n = 1–15). In addition, we observed protonated mixed cluster ions of $[(CH_3OH)_n(H_2O) + H]^+$ (n = 1–11) and $[(CH_3OH)_n(CH_3OCH_3) + H]^+$ (n = 1–3) between the $[(CH_3OH)_n + H]^+$ peaks. Andrade et al. reported an intense series of $(CH_3OH)_nHCO^+$ (n = 1–7) in secondary ions from methanol ice surfaces by ^{252}Cf fission fragments.[3] However, we did not observe these ions under the present experimental conditions. $[(CH_3OH)_n(H_2O) + H]^+$ were suggested to form by elimination of dimethyl ether (CH_3OCH_3) from protonated methanol clusters:[29–32]

$$[(CH_3OH)_{n+2} + H]^+ \rightarrow [(CH_3OH)_n(H_2O) + H]^+ + CH_3OCH_3 \quad (7)$$

This reaction proceeds with high probability when the cluster size n >6.[29–32] The present results are consistent with this tendency, exhibiting a distribution of $[(CH_3OH)_n(H_2O) + H]^+$ with a maximum ca. n = 9. $[(CH_3OH)_n(CH_3OCH_3) + H]^+$ (n = 1–3) can form by dehydration (i.e., H_2O loss) from protonated methanol clusters:[31]

$$[(CH_3OH)_{n+2} + H]^+ \rightarrow [(CH_3OH)_n(CH_3OCH_3) + H]^+ + H_2O \quad (8)$$

3.1.2 Positive fragment and reaction product ions

Figure 1(b) focuses on a low-mass range of the mass spectrum. In a previous study, a large number of background ions from the gas-phase molecules prevented us from identifying the low-mass positive ions.[27] In this study, we could eliminate the background ions because of the coincidence method. As a result, we identified H^+, H_2^+, C^+, CH_i^+ (i = 0–3), H_3O^+, CHO^+, and CH_2OH^+ as the fragment ions emitted from the droplet surface.

A previous study for ethanol droplets[26] indicates that singly charged parent ions dissociate post-protonation by rapid proton transfer. Similar processes are expected for methanol droplets; namely, fragmentation through protonated methanol $CH_3OH_2^+$. The dissociation pathways of $CH_3OH_2^+$ were suggested in studies of collision-induced dissociation, as follows:[33–36]

$$CH_3OH_2^+ \rightarrow CH_3^+ + H_2O \quad (9)$$

$$CH_3OH_2^+ \rightarrow CH_2OH^+ + H_2 \quad (10)$$

H^+, H_2^+, and C^+ are not produced during $CH_3OH_2^+$ dissociation.[33] Furthermore, in the electron impact fragmentation of gas-phase methanol, H^+ was not reported, and the yields of H_2^+ and C^+ were negligibly small.[37] However, production of these ions was confirmed in fast heavy ion collisions with gas-phase methanol (Figure 2). Thus, we suggest that H^+, H_2^+, and C^+ are emitted directly by Coulomb explosion of multiply charged parent ions on the droplet surface. We confirm that H^+ and H_2^+ have kinetic energies (KEs) of ~10 eV, estimated from the TOF peak width (Figure 3). C^+ has a KE of ~5 eV, although the statistics were not sufficiently high for precise evaluation. This KE value is consistent with those in dissociation from multiple-ionized acetylene C_2H_2 (~7 eV) and ethylene C_2H_4 (~5 eV).[38,39]

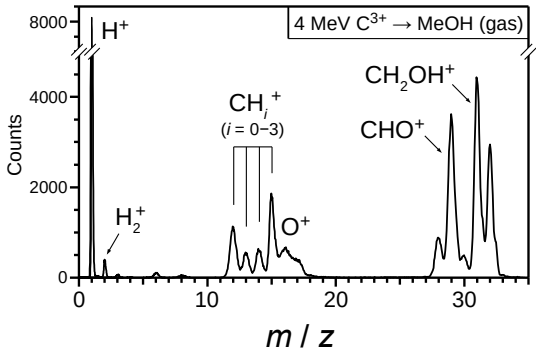

Figure 2. TOF spectrum of product ions from gas-phase methanol by 4-MeV C^{3+} collisions (unpublished results).

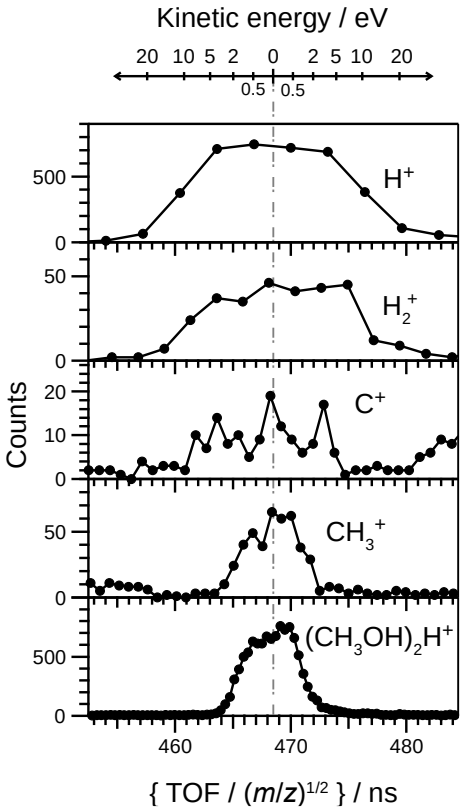

Figure 3. TOF peaks of H^+, H_2^+, C^+, CH_3^+, and $[(CH_3OH)_2 + H]^+$. The horizontal axis is TOF divided by the square root of each corresponding m/z. The upper axis represents the kinetic energy of the ions.

We observed secondary reaction product ions $C_2H_7O^+$ (m/z = 47) and $C_2H_5O^+$ (m/z = 45). $C_2H_7O^+$ is supposed to be a protonated dimethyl ether $(CH_3OCH_3)H^+$ produced from a protonated dimer $(CH_3OH)_2H^+$ by dehydration (8).[29–32,40,41]

3.2 Negative ions

Figure 4 shows the mass spectra of the negative secondary ions emitted from the CH_3OH droplets. The vertical and horizontal axes represent the relative intensity and m/z of the secondary ions, respectively, as in Figure 1. We compared the results for CH_3OD droplets with CH_3OH (Figure 5). The deuterated peaks shifted to the high-mass side. Concomitantly, some peaks did not shift when they had no D atoms. Table 2 shows the secondary ion yields evaluated from both spectra. Negative ions are emitted with the same order of probability as positive ions, indicating that negative ions are efficiently produced by deprotonation. Section 3.3 discusses in detail the mechanism that generates various reaction product ions.

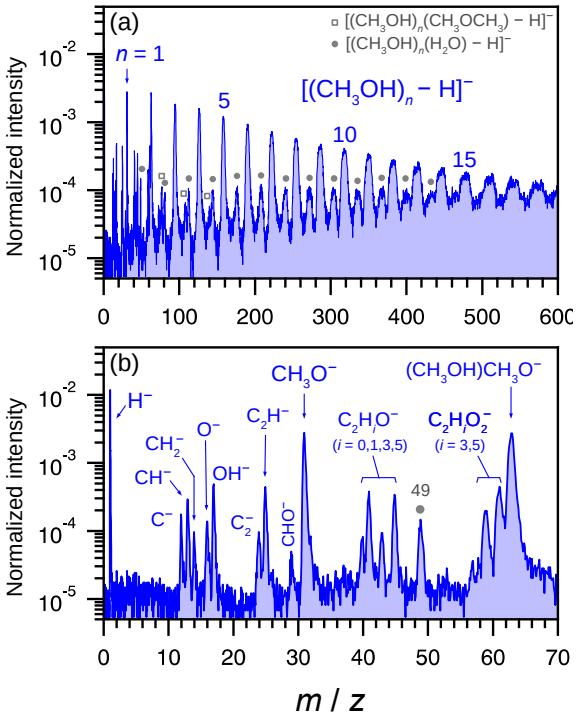

Figure 4. (a) and (b) Mass spectra plotted as in Figure 1 for negative secondary ions.

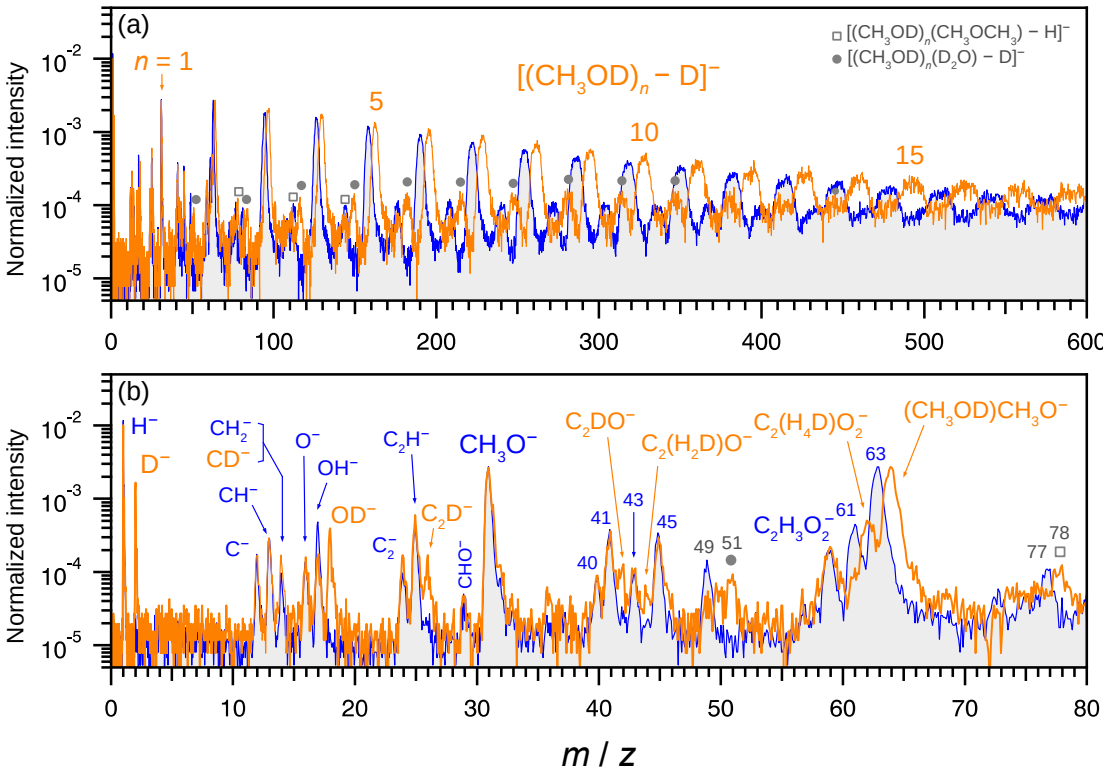

Figure 5. (a) Comparisons of mass spectra for negative secondary ions emitted from droplets of CH_3OD (orange line) and CH_3OH (blue line filled with gray). (b) Expanded mass spectra in the range of m/z <80. The vertical and horizontal axes are the same as in Figure 1.

Table 2. Negative secondary ion yields emitted from CH_3OH and CH_3OD droplets per single 2.0-MeV C^{2+} impact.[a]

m/z	CH_3OH droplets		CH_3OD droplets	
	Negative ions	Ion yields per impact ($\times 10^{-2}$)	Negative ions	Ion yields per impact ($\times 10^{-2}$)
1	H^-	7.17	H^-	5.33
2			D^-	1.05
12	C^-	0.18	C^-	0.22

13	CH^-	0.39	CH^-	0.39
14	CH_2^-	0.09	CH_2^- and CD^-	0.22
16	O^-	0.20	O^-	0.21
17	OH^-	0.54	OH^-	0.23
18			OD^-	0.42
24	C_2^-	0.12	C_2^-	0.20
25	C_2H^-	0.52	C_2H^-	0.69
26			C_2D^-	0.20
29	CHO^-	0.04	CHO^-	0.04
31	CH_3O^-	3.63	CH_3O^-	3.89
40	C_2O^-	0.10	C_2O^-	0.12
41	C_2HO^-	0.48	C_2HO^-	0.45
42			C_2DO^-	0.13
43	$C_2H_3O^-$	0.12	$C_2H_3O^-$	0.13
44			$C_2(H_2D)O^-$	0.05
45	$C_2H_5O^-$	0.42	$C_2H_5O^-$	0.45
49	$[(CH_3OH)(H_2O) - H]^-$	0.19	$[(CH_3OD)(H_2O) - D]^-$	0.04
50			$[(CH_3OD)(HDO) - D]^-$	0.07
51			$[(CH_3OD)(D_2O) - D]^-$	0.13
59	$C_2H_3O_2^-$	0.39	$C_2H_3O_2^-$	0.56
61	$C_2H_5O_2^-$	0.90		
62			$C_2(H_4D)O^-$	1.14
	$[(CH_3OH)_n - H]^-$		$[(CH_3OD)_n - D]^-$	
	$n = 2$	5.71	$n = 2$	6.23
	$n = 3$	7.73	$n = 3$	8.99
	$n = 4$	7.25	$n = 4$	8.64
	$n = 5$	5.84	$n = 5$	6.85

	$n = 6$	5.08	$n = 6$	6.10
	$n = 7$	4.51	$n = 7$	5.55
	$n = 8$	3.85	$n = 8$	4.75
	$n = 9$	3.42	$n = 9$	4.19
	$n = 10$	3.06	$n = 10$	3.61
	$n = 11$	2.75	$n = 11$	3.30
	$n = 12$	2.36	$n = 12$	2.68
	$n = 13$	2.15	$n = 13$	2.57
	$n = 14$	1.97	$n = 14$	2.36
	Total	71.2	Total	82.2

[a] We did not evaluate the values for the mixed clusters because of the large uncertainties.

3.2.1 Negative cluster ions

We observed deprotonated cluster ions $[(CH_3OH)_n - H]^-$ or its deuterated species $[(CH_3OD)_n - D]^-$ (n = 1–21) as the dominant negative ions. Similarly to the positive ions, we observed mixed clusters of $[(CH_3OH)_n(H_2O) - H]^-$ (n = 1–13) and $[(CH_3OH)_n(CH_3OCH_3) - H]^-$ (n = 1–3) for CH_3OH droplets. For CH_3OD droplets, $[(CH_3OD)_n(D_2O) - D]^-$ and $[(CH_3OD)_n(CH_3OCH_3) - H]^-$ seem to be dominant (as deduced from the peak at m/z = 51 and 78 for n = 1, respectively), although it is difficult to distinguish the H^+ or D^+ loss in larger clusters because of insufficient mass resolution. The origin of the water molecule in $[(CH_3OH)_n(H_2O) - H]^-$ could be contaminated water molecules, as suggested by Kosevich et al. in experiments of 15-keV Cs^+ irradiation on methanol ice.[42] However, mainly D_2O or OD^-, rather than absorbed H_2O or OH^-, are involved in the case of the present CH_3OD droplet measurement. Therefore, the origins of the mixed water molecules in the present experiments seem to be fragments (OH^- and OD^-) or products of CH_3OCH_3 elimination from deprotonated clusters.

3.2.2 Negative fragment ions

Fragment anions generated from CH_3OH droplets were H^-, CH_i^- (i = 0–2), OH_i^- (i = 0, 1), and CH_iO^- (i = 1, 3) [Figure 4(b)]. Fragment anion species were mostly those observed in the electron-induced fragmentation of gas-phase methanol at the collision energy of 70 eV,[20,21] although the intensity distributions were completely different. H^-, O^-, OH^-, and CH_3O^- might have also been produced by DEA.[18,19] In low-energy electron-induced reactions on a methanol ice surface, CH_i^- (i = 1–3) was proposed to be generated by secondary reactions of H^- with neighboring methanol molecules.[8] However, CH_3^- was absent in the present experiments. The reason for the difference is unclear.

In the spectra of CH_3OD droplets [Figure 5(b)], peaks of fragment ions containing a D atom were evident. The peak intensity at m/z = 14 increased because of CD^- production. The CH_3O^- peak was almost unchanged. Thus, most H^+ or D^+ desorption occurred from the hydroxy group. Note that OH^- was still present, even for CH_3OD droplets. OH^- can be formed by hydrogen scrambling, which was reported in electron-induced fragmentation[21] and DEA[18] to gas-phase CH_3OD, or secondary reactions of O^- with a neighboring methanol molecule.[8]

3.3 Negative reaction product ions

Formation of product ions containing two carbon atoms requires secondary reactions that involve two methanol molecules. We observed a richer variety of reaction product ions compared with positive ions; i.e., $C_2H_i^-$ (i = 0, 1), $C_2H_iO^-$ (i = 0, 1, 3, 5), and $C_2H_iO_2^-$ (i = 3, 5). In a previous study for ethanol droplets, we observed hydrocarbon anions such as C_3^-, C_3H^-, $C_3H_2^-$, C_4^-, and C_4H^-.[24] They are considered to be produced by chemical reactions associated

with a nanoplasma state in a heavy ion track.[43] For methanol droplets, C_2^- and C_2H^- might be generated by similar processes. At present, it is difficult to discuss the formation mechanism of C_2^- and C_2H^- in more detail because of the lack of experimental clues to investigate the mechanism. In the following sections, we discuss the formation processes of $C_2H_iO_2^-$ (i = 3, 5) and $C_2H_iO^-$ (i = 1, 3, 5) based on comparing the results for CH_3OH and CH_3OD droplets.

3.3.1. $C_2H_5O_2^-$ (m/z = 61) and $C_2(H_4D)O_2^-$ (m/z = 62)

Before considering $C_2H_5O_2^-$ at m/z = 61, recall that the peak of the deprotonated dimer $[(CH_3OH)_2 - H]^-$, or $(CH_3OH)CH_3O^-$, at m/z = 63 shifted by 1 as the result of deuteration into $[(CH_3OD)_2 - D]^-$, or $(CH_3OD)CH_3O^-$ in the CH_3OD spectrum. The peak of $C_2H_5O_2^-$ at m/z = 61 similarly shifted by 1 for CH_3OD droplets. Thus, we assigned the peak at m/z = 62 to be $(CH_3OD)CHO^-$ generated from $(CH_3OD)CH_3O^-$ by H_2 elimination rather than HD elimination.

3.3.2. $C_2H_3O_2^-$ (m/z = 59)

In contrast, the peak at m/z = 59 did not shift even for CH_3OD droplets, indicating that the corresponding reaction product has no D atom. Therefore, we assigned this peak to $C_2H_3O_2^-$, also in the spectrum of CH_3OD droplets. To explain the production of $C_2H_3O_2^-$ from CH_3OD droplets, here we suggest an association reaction between CH_3O^- and neutral CO:

$$CH_3O^- + CO \rightarrow C_2H_3O_2^- \quad (11)$$

CH_3O^- is the most abundant fragment anion. CO is a major neutral fragments reported in a MeV-energy heavy ion irradiation study on methanol ice.[4] Note that this reaction does not involve D atoms, even for CH_3OD.

As another possible mechanism, here we verify the possibility of DEA to neutral $C_2H_4O_2$, which might be produced by radical–radical reactions. Production of methyl formate (CH_3OCHO) was reported in a study of MeV-energy heavy ion irradiation on methanol ice.[4] The DEA to methyl formate is likely to produce more CHO^- than $C_2H_3O_2^-$.[44] In the present experiments, the CHO^- yield was much less than that of $C_2H_3O_2^-$. Thus, DEA to methyl formate negligibly contributed to the present experiments. In the study of DEA to acetic acid (CH_3COOH), which is a structural isomer of CH_3OCHO, Sailer et al. observed formation of $CH_2O_2^-$ (m/z = 46) with a similar intensity as $C_2H_3O_2^-$.[45] In the present experiments, DEA to acetic acid can be excluded because of the absence of the peak at m/z = 46 (Figure 2). The other possible isomer is glycolaldehyde ($HOCH_2CHO$). However, de Barros et al. did not observe glycolaldehyde in MeV-energy heavy ion irradiation on methanol ice.[4] Furthermore, selective production of $C_2H_3O_2^-$ without D atoms seems difficult in radical–radical reactions because CH_2OD should be involved in radical reactions. For these reasons, we conclude that DEA to neutral reaction products plays a minor role in forming $C_2H_3O_2^-$ in the present experiments. Again, the absence of the D atom is attributable to the CH_3O^- and CO reaction.

Regarding the structure of $C_2H_3O_2^-$, a deprotonated form of methyl formate (methoxymethanone, CH_3OCO^-) is the first candidate. Methyl formate is a neutral product in MeV-energy heavy ion irradiation on methanol ice.[4] CH_3OCO^- has a straightforward structure, formed by association of CH_3O^- with CO. To confirm the possibility of the association reaction, we evaluated the total energy of the two-molecule system of CH_3O^- and CO, as a function of the O atom of CH_3O and the C atom of CO. We confirmed that the constructed potential curve exhibited no energy barrier (Figure S1 in the Supporting Information). This result indicates a pathway that has no barrier in this reaction. Furthermore, we evaluated the binding energy of

CH_3OCO^- (i.e., the difference in the energies before and after the reaction) to be only 0.526 eV. Further isomerization might be possible near the projectile trajectory because of high electronic excitation. We found acetate anion (CH_3COO^-) and hydroxymethylcarbonyl anion (OCH_2CHO^-) as additional candidates for $C_2H_3O_2^-$. The binding energies of CH_3COO^- and OCH_2CHO^- were calculated to be ca. 2.76 and 0.702 eV, respectively. We found a reaction pathway leading to CH_3COO^- from CH_3OCO^-, with the transition state expressed as $[CH_3\cdots CO_2]^-$:

$$CH_3OCO^- \rightarrow [CH_3\cdots CO_2]^- \rightarrow CH_3COO^- \quad (12)$$

The energy barrier was 1.94 eV relative to the initial state of CH_3O^- + CO, which might be overcome by a high energy density around the ion track. We did not find the reaction pathway leading to OCH_2CHO^- in our calculations. Figure 6 shows the energy levels and optimized geometries. Sekiguchi and Uggerud reported an energy diagram connecting CH_3O^- + CO and some different forms of deprotonated glycolaldehyde, with binding energies in the 0.56- to 0.93-eV range,[46] which are also candidates for $C_2H_3O_2^-$.

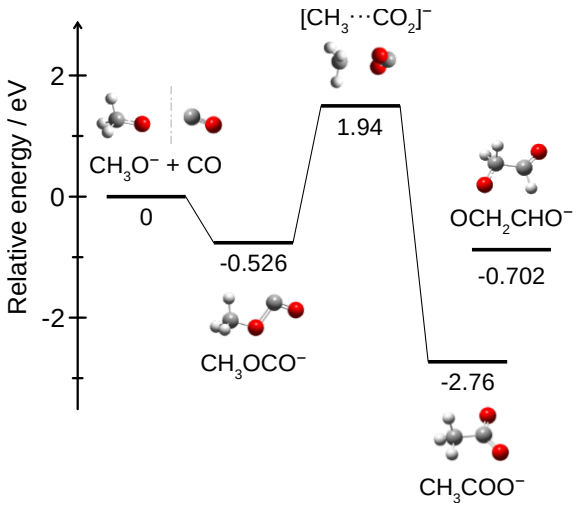

Figure 6. Potential energy levels of $C_2H_3O_2^-$ relative to the initial state of CH_3O^- + CO.

3.3.3. $C_2H_5O^-$ (m/z = 45)

We assigned $C_2H_5O^-$ to be deprotonated dimethyl ether (methanidyloxymethane, $CH_3OCH_2^-$), produced by dehydration of deprotonated dimer anions $[(CH_3OH)_2 - H]^-$, similarly to the case of protonated dimethyl ether (Section 3.1.1). Note that the results for the CH_3OD droplets exhibited a negligible or small yield of $C_2(H_4D)O^-$ (m/z = 46) compared with the yield of $C_2H_5O^-$. This indicates that the dehydration proceeded using the D atom of the hydroxy group:

$$[(CH_3OD)_2 - D]^- \text{ [or } (CH_3OD)\ CH_3O^-] \rightarrow CH_3OCH_2^- + HDO \quad (13)$$

3.3.4. $C_2H_3O^-$ (m/z = 43) and $C_2(H_2D)O^-$ (m/z = 44)

In the CH_3OD spectra, a peak at m/z = 44 was evident with an intensity of ca. 40% of $C_2H_3O^-$ (m/z = 43). We assigned this peak to be $C_2(H_2D)O^-$, in which a D atom replaces an H atom of $C_2H_3O^-$. $C_2(H_2D)O^-$ cannot be produced by H_2 or 2H loss from $C_2H_5O^-$, whereas $C_2(H_4D)O^-$ was absent. Thus, we propose the following association reactions between fragment anions and neutral species as a different mechanism:

$$C^- + CH_2OH \rightarrow C_2H_3O^- \quad (14)$$

$$CH^- + CH_2O \rightarrow C_2H_3O^- \quad (15)$$

$$CH_2^- + CHO \rightarrow C_2H_3O^- \quad (16)$$

We observed substantial quantities of C^-, CH^-, and CH_2^- in the present measurements. Neutral fragments of CH_2OH, CH_2O, and CHO were reported in a study of frozen methanol.[4] In these reactions, a D atom can be included in the anion or neutral fragments. We confirmed that the

potential curves regarding reactions (14)–(16) as a function of the C–C distance exhibited no energy barrier (Figure S2).

3.3.5. C_2HO^- (m/z = 41) and C_2DO^- (m/z = 42)

In the same manner as $C_2H_3O^-$, production of C_2HO^- can be explained by association reactions, as follows:

$$C^- + CHO \rightarrow C_2HO^- \quad (17)$$

$$CH^- + CO \rightarrow C_2HO^- \quad (18)$$

We confirmed that these association reactions also had no barrier (Figure S3). Figure 7 shows the energy levels concerning reactions (14)–(18). In addition to reactions (17) and (18), C_2HO^- can be produced by subsequent H_2 loss from $C_2H_3O^-$ after reactions (14)–(16) because of the considerable excess energies in the reactions.

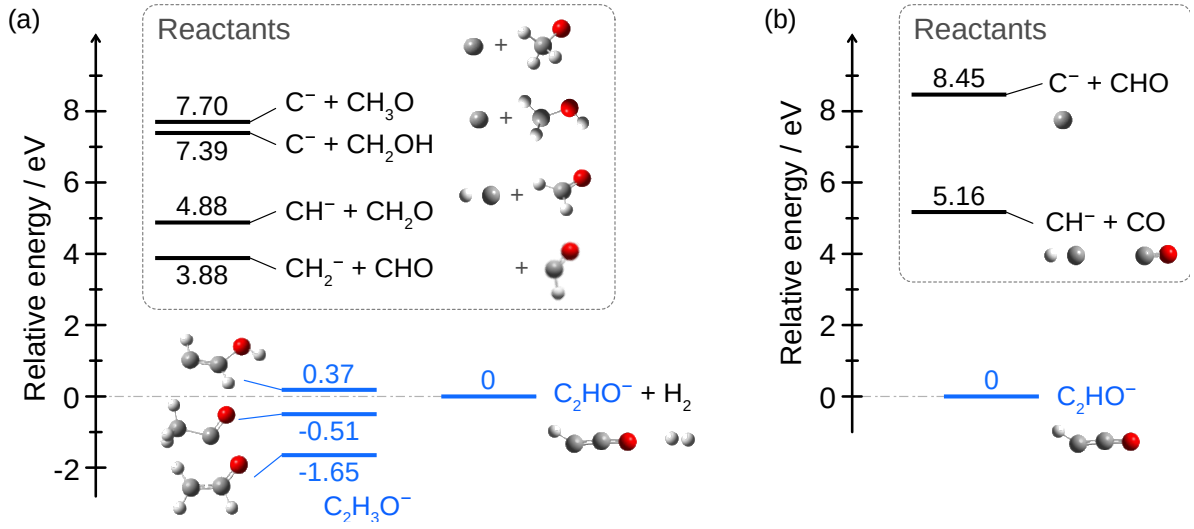

Figure 7. Energy levels regarding the association reactions into (a) $C_2H_3O^-$ and (b) C_2HO^-.

4. SUMMARY

To evaluate complex reaction processes that form positive and negative ionic products by MeV-energy heavy ion irradiation in condensed matter, we performed a mass spectrometric study of secondary ions emitted from methanol microdroplet surfaces by 2.0-MeV C^{2+} irradiation. The present mass spectrometric study, using the droplet target in high vacuum, enabled precise, systematic comparisons of complex positive and negative ion species generated on fresh surfaces without contamination. In particular, coincidence measurements with forward-scattered projectiles enabled selective observation of secondary ions that originated from the droplet surface and quantitative analysis of the secondary ion yields. Comparisons between the positive and negative secondary ions clearly indicate that the negative ions tend to form a larger variety of product ions.

We compared the mass spectra of the negative secondary ions obtained from CH_3OH with CH_3OD droplets to reveal the formation processes of the various secondary reaction product ions. These results provided evidence of the important role of association reactions of anion fragments with neutral fragments. For example, $C_2H_3O_2^-$ at m/z = 59 was produced by CH_3O^- and CO, based on the result that this product ion did not contain a D atom. We also suggested that $C_2H_3O^-$ (m/z = 43) and C_2HO^- (m/z = 41) formed by association reactions between fragment anions of CH_i^- (i = 0–2) and neutral species of CH_jO (j = 0–3). Quantum chemical calculations confirm that these reactions can proceed without energy barriers.

The important point is that these reactions proceeded in the sub-nanosecond time scale of ion emission from the surface. Therefore, the reactants must be originally produced close to each other in high density because there is insufficient time to diffuse and find a reaction partner before such a rapid ion emission. In fast heavy-ion collisions, a large number of fragments are

produced within each ion track generated by a single ion penetration. A reaction field containing a high density of fragments is formed by single-ion impact. It is known that radical–radical reactions are enhanced in high linear energy transfer radiation. The present study proposes that anion–molecule reactions among fragments are similarly activated in fast heavy-ion-induced reactions, and play an important role in generating complex product ions as the unique mechanism enabled by fast heavy ion collisions in condensed matter.

ASSOCIATED CONTENT

Supporting Information

Potential energy curves of the two-molecule systems regarding anion–molecule reactions among fragments (PDF).

AUTHOR INFORMATION

Corresponding Author

Takuya Majima – Department of Nuclear Engineering, Kyoto University, Kyoto 615-8540, Japan; orcid.org/0000-0003-2804-1915; Email: majima@nucleng.kyoto-u.ac.jp

Notes

The authors declare no competing financial interest.

ACKNOWLEDGMENT

This work was supported by JSPS KAKENHI (Grant No. 21H01055), The Kyoto University Foundation, ISHIZUE 2020 of Kyoto University Research Development Program, and the Kansai atomic conference (KANGENKON). We acknowledge Mr. Masahiro Naito and Mr. Yoshitaka Sasaki for providing technical support during experiments. We are grateful for use of the HOKUSAI-GreatWave supercomputer system of RIKEN and the supercomputer of ACCMS, Kyoto University. T.M. gratefully acknowledges Dr. Yoichi Nakai and Atsuki Ishibashi for helpful discussions. We thank Michael Scott Long, PhD, from Edanz (https://jp.edanz.com/ac) for editing a draft of this manuscript.

REFERENCES

(1) Schardt, D.; Elsässer, T.; Schulz-Ertner, D. Heavy-Ion Tumor Therapy: Physical and Radiobiological Benefits. *Rev. Mod. Phys.* **2010**, *82*, 383–425. https://doi.org/10.1103/RevModPhys.82.383.

(2) Bringa, E. M.; Johnson, R. E. In *Solid State Astrochemistry*; Springer Netherlands: Dordrecht, 2003; pp 357–393. https://doi.org/10.1007/978-94-010-0062-8_11.

(3) Andrade, D. P. P.; Boechat-Roberty, H. M.; Martinez, R.; Homem, M. G. P.; da Silveira, E. F.; Rocco, M. L. M. Frozen Methanol Bombarded by Energetic Particles: Relevance to Solid State Astrochemistry. *Surf. Sci.* **2009**, *603*, 1190–1196. https://doi.org/10.1016/j.susc.2009.02.035.

(4) de Barros, A. L. F.; Domaracka, A.; Andrade, D. P. P.; Boduch, P.; Rothard, H.; da Silveira, E. F. Radiolysis of Frozen Methanol by Heavy Cosmic Ray and Energetic Solar Particle Analogues. *Mon. Not. R. Astron. Soc.* **2011**, *418*, 1363–1374. https://doi.org/10.1111/j.1365-2966.2011.19587.x.

(5) Rothard, H.; Domaracka, A.; Boduch, P.; Palumbo, M. E.; Strazzulla, G.; da Silveira, E. F.; Dartois, E. Modification of Ices by Cosmic Rays and Solar Wind. *J. Phys. B: At., Mol. Opt. Phys.* **2017**, *50*, 062001. https://doi.org/10.1088/1361-6455/50/6/062001.

(6) Dartois, E.; Chabot, M.; Id Barkach, T.; Rothard, H.; Augé, B.; Agnihotri, A. N.; Domaracka, A.; Boduch, P. Non-Thermal Desorption of Complex Organic Molecules. *Astron. Astrophys.* **2019**, *627*, A55. https://doi.org/10.1051/0004-6361/201834787.

(7) Almeida, G. C.; Andrade, D. P. P.; Arantes, C.; Nazareth, A. M.; Boechat-Roberty, H. M.; Rocco, M. L. M. Desorption from Methanol and Ethanol Ices by High Energy Electrons: Relevance to Astrochemical Models. *J. Phys. Chem. C* **2012**, *116*, 25388–25394. https://doi.org/10.1021/jp308680k.

(8) Boyer, M. C.; Boamah, M. D.; Sullivan, K. K.; Arumainayagam, C. R.; Bazin, M.; Bass, A. D.; Sanche, L. Dynamics of Dissociative Electron–Molecule Interactions in Condensed Methanol. *J. Phys. Chem. C* **2014**, *118*, 22592–22600. https://doi.org/10.1021/jp506365d.

(9) Friedman, L.; Long, F. A.; Wolfsberg, M. Study of the Mass Spectra of the Lower Aliphatic Alcohols. *J. Chem. Phys.* **1957**, *27*, 613–622. https://doi.org/10.1063/1.1743799.

(10) Spinks, J. W. T.; Woods, R. J. Organic Compounds. In *An introduction to radiation chemistry*; John Wiley and Sons Inc: New York, 1990; pp 364–451.

(11) Dainton, F. S.; Salmon, G. A.; Wardman, P. The Radiation Chemistry of Liquid and Glassy Methanol. *Proc. R. Soc. A* **1969**, *313*, 1–30. https://doi.org/10.1098/rspa.1969.0177.

(12) Baxendale, J. H.; Wardman, P. *The Radiolysis of Methanol: Product Yields, Rate Constants, and Spectroscopic Parameters of Intermediates*; Gaithersburg, MD, 1975; Vol. 54. https://doi.org/10.6028/NBS.NSRDS.54.

(13) Johnson, D. W.; Salmon, G. A. The Effects of Dose and Base on the Lifetime of Es- in Pulse Irradiated Methanol: The Reaction of Es- with Hydroxymethyl Radicals. *Radiat. Phys. Chem.* **1977**, *10*, 294–296. https://doi.org/10.1016/0146-5724(77)90033-4.

(14) Saenko, E. v.; Feldman, V. I. Radiation-Induced Transformations of Methanol Molecules in Low-Temperature Solids: A Matrix Isolation Study. *Phys. Chem. Chem. Phys.* **2016**, *18*, 32503–32513. https://doi.org/10.1039/C6CP06082J.

(15) Li, Z.; Fu, C.-F.; Chen, Z.; Tong, T.; Hu, J.; Yang, J.; Tian, S. X. Electron-Induced Synthesis of Dimethyl Ether in the Liquid–Vapor Interface of Methanol. *J. Phys. Chem. Lett.* **2022**, 5220–5225. https://doi.org/10.1021/acs.jpclett.2c00787.

(16) Majima, T.; Murai, T.; Kishimoto, T.; Adachi, Y.; Yoshida, S. O.; Tsuchida, H.; Itoh, A. Correlation between Multiple Ionization and Fragmentation of C_2H_6 in Charge-Changing Collisions with 580-keV C^+. *Phys. Rev. A* **2014**, *90*, 062711. https://doi.org/10.1103/PhysRevA.90.062711.

(17) De, S.; Rajput, J.; Roy, A.; Ahuja, R.; Ghosh, P. N.; Safvan, C. P. Dissociation of Methanol and Acetylene by Slow Highly Charged Ion Collision. *J. Phys.: Conf. Ser.* **2007**, *80*, 012005. https://doi.org/10.1088/1742-6596/80/1/012005.

(18) Kühn, A.; Fenzlaff, H.; Illenberger, E. Formation and Dissociation of Negative Ion Resonances in Methanol and Allylalcohol. *J. Chem. Phys.* **1988**, *88*, 7453–7458. https://doi.org/10.1063/1.454309.

(19) Ibănescu, B. C.; May, O.; Monney, A.; Allan, M. Electron-Induced Chemistry of Alcohols. *Phys. Chem. Chem. Phys.* **2007**, *9*, 3163–3173. https://doi.org/10.1039/B704656A.

(20) Melton, C. E.; Rudolph, P. S. Negative Ion Mass Spectra of Hydrocarbons and Alcohols. *J. Chem. Phys.* **1959**, *31*, 1485–1488. https://doi.org/10.1063/1.1730641.

(21) Thynne, J. C. J. The Negative Ion Mass Spectra of Methanol and Deuterated Methanol. *Org. Mass Spectrom.* **1973**, *7*, 899–901. https://doi.org/10.1002/oms.1210070715.

(22) Andrade, D. P. P.; Rocco, M. L. M.; Boechat-Roberty, H. M. X-Ray Photodesorption from Methanol Ice. *Mon. Not. R. Astron. Soc.* **2010**, *409*, 1289–1296. https://doi.org/10.1111/j.1365-2966.2010.17395.x.

(23) Majima, T.; Kitajima, K.; Nishio, T.; Tsuchida, H.; Itoh, A. Secondary Ion Emission from Ethanol Microdroplets Induced by Fast Heavy Ions. *J. Phys.: Conf. Ser.* **2015**, *635*, 012021. https://doi.org/10.1088/1742-6596/635/1/012021.

(24) Kitajima, K.; Majima, T.; Nishio, T.; Oonishi, Y.; Mizutani, S.; Kohno, J.; Saito, M.; Tsuchida, H. Mass Spectrometric Study of the Negative and Positive Secondary Ions Emitted from Ethanol Microdroplets by MeV-Energy Heavy Ion Impact. *Nucl. Instrum. Methods Phys. Res., Sect. B* **2018**, *424*, 10–16. https://doi.org/10.1016/j.nimb.2018.03.029.

(25) Sunner, J. Ionization in Liquid Secondary Ion Mass Spectrometry (LSIMS). *Org. Mass Spectrom.* **1993**, *28*, 805–823. https://doi.org/10.1002/oms.1210280802.

(26) Majima, T.; Mizutani, S.; Mizunami, Y.; Kitajima, K.; Tsuchida, H.; Saito, M. Fast-Ion-Induced Secondary Ion Emission from Submicron Droplet Surfaces Studied Using a New Coincidence Technique with Forward-Scattered Projectiles. *J. Chem. Phys.* **2020**, *153*, 224201. https://doi.org/10.1063/5.0032301.

(27) Kitajima, K.; Tsuchida, H.; Majima, T.; Saito, M. Effects of Electronic Stopping Power on Fast-Ion-Induced Secondary Ion Emission from Methanol Microdroplets. *Eur. Phys. J. D* **2018**, *72*, 169. https://doi.org/10.1140/epjd/e2018-90218-4.

(28) Frisch, M. J.; Trucks, G. W.; Schlegel, H. B.; Scuseria, G. E.; Robb, M. A.; Cheeseman, J. R.; Scalmani, G.; Barone, V.; Petersson, G. A.; Nakatsuji, H. et al. Gaussian16 Revision C.01. Gaussian, Inc.: Wallingford CT 2016.

(29) Morgan, S.; Keesee, R. G.; Castleman, A. W. Reactions of Methanol Clusters Following Multiphoton Ionization. *J. Am. Chem. Soc.* **1989**, *111*, 3841–3845. https://doi.org/10.1021/ja00193a014.

(30) Zhang, X.; Yang, X.; Castleman, A. W. Study of Protonated Methanol Cluster Ions under Thermal Conditions. *Chem. Phys. Lett.* **1991**, *185*, 298–302. https://doi.org/10.1016/S0009-2614(91)85063-3.

(31) El-Shall, M. S.; Marks, C.; Sieck, L. W.; Meot-Ner, M. Reactions and Thermochemistry of Protonated Methanol Clusters Produced by Electron Impact Ionization. *J. Phys. Chem.* **1992**, *96*, 2045–2051. https://doi.org/10.1021/j100184a007.

(32) Bandyopadhyay, B.; Kostko, O.; Fang, Y.; Ahmed, M. Probing Methanol Cluster Growth by Vacuum Ultraviolet Ionization. *J. Phys. Chem. A* **2015**, *119*, 4083–4092. https://doi.org/10.1021/acs.jpca.5b00912.

(33) Bowers, M. T.; Chesnavich, W. J.; Huntress, W. T. Deactivation of Internally Excited H_3^+ Ions: Comparison of Experimental Product Distributions of Reactions of H_3^+ Ions with CH_3NH_2, CH_3OH and CH_3SH with Predictions of Quasiequilibrium Theory Calculations. *Int. J. Mass Spectrom. Ion Phys.* **1973**, *12*, 357–382. https://doi.org/10.1016/0020-7381(73)80105-6.

(34) Fiaux, A.; Smith, D. L.; Futrell, J. H. Thermal Energy Reactions of H_3^+ with Methanol. *Int. J. Mass Spectrom. Ion Phys.* **1976**, *20*, 223–235. https://doi.org/10.1016/0020-7381(76)80151-9.

(35) Day, R. J.; Krause, D. A.; Jorgensen, W. L.; Cooks, R. G. Energy Partitioning Accompanying Fragmentation of Protonated Methanol. *Int. J. Mass Spectrom. Ion Phys.* **1979**, *30*, 83–92. https://doi.org/10.1016/0020-7381(79)80045-5.

(36) Nobes, R. H.; Radom, L. The Structure and Dissociation Pathways of Protonated Methanol: Anab Initio Molecular Orbital Study. *Org. Mass Spectrom.* **1982**, *17*, 340–344. https://doi.org/10.1002/oms.1210170711.

(37) Wallace, W. E., Mass Spectra in *NIST Chemistry WebBook;* Linstrom, P. J., Mallard W.G., Eds; NIST Standard Reference Database Number 69; National Institute of Standards and Technology: Gaithersburg, MD, http://webbook.nist.gov, (retrieved July 21, 2022).

(38) Yoshida, S.; Majima, T.; Asai, T.; Matsubara, M.; Tsuchida, H.; Saito, M.; Itoh, A. Kinetic Energy Distributions of Product Ions from Singly and Multiply Ionized C_2H_2 Molecules Induced by 0.8 MeV C^+ Collisions. *Nucl. Instrum. MethodsPhys. Res., Sect. B* **2017**, *408*, 203–208. https://doi.org/10.1016/j.nimb.2017.03.100.

(39) Yoshida, S.; Majima, T.; Tsuchida, H.; Saito, M. Kinetic Energy Distributions of the Fragment Ions from Multiply Ionized C_2H_6 as Functions of the Charge State of the Intermediate States. *X-Ray Spectrom.* **2020**, *49*, 177–183. https://doi.org/10.1002/xrs.3084.

(40) Morgan, S.; Castleman, A. W. Evidence of Delayed Internal Ion-Molecule Reactions Following the Multiphoton Ionization of Clusters: Variation in Reaction

Channels in Methanol with Degree of Solvation. *J. Am. Chem. Soc.* **1987**, *109*, 2867–2870. https://doi.org/10.1021/ja00244a001.

(41) Mafuné, F.; Kohno, J.; Kondow, T. Ion−Molecule Reactions in a Liquid Beam of Methanol, Ethanol, and 1-Propanol Following Multiphoton Ionization. *J. Phys. Chem.* **1996**, *100*, 10041–10045. https://doi.org/10.1021/jp953603j.

(42) Kosevich, M. v.; Czira, G.; Boryak, O. A.; Shelkovsky, V.; Vekey, K. Comparison of Positive and Negative Ion Clusters of Methanol and Ethanol Observed by Low Temperature Secondary Ion Mass Spectrometry. *Rapid Commun. Mass Spectrom.* **1997**, *11*, 1411–1416. https://doi.org/https://doi.org/10.1002/(SICI)1097-0231(19970830)11:13%3C1411::AID-RCM967%3E3.0.CO;2-8.

(43) Wagner, M.; Wien, K.; Curdes, B.; Hilf, E. R. Secondary Ion Emission from Frozen Alkanes and Benzene Induced by MeV-Ion Impact. *Nucl. Instrum. MethodsPhys. Res., Sect. B* **1993**, *82*, 362–378. https://doi.org/10.1016/0168-583X(93)96041-A.

(44) Feketeová, L.; Pelc, A.; Ribar, A.; Huber, S. E.; Denifl, S. Dissociation of Methyl Formate ($HCOOCH_3$) Molecules upon Low-Energy Electron Attachment. *Astron. Astrophys.* **2018**, *617*, A102. https://doi.org/10.1051/0004-6361/201732293.

(45) Sailer, W.; Pelc, A.; Probst, M.; Limtrakul, J.; Scheier, P.; Illenberger, E.; Märk, T. D. Dissociative Electron Attachment to Acetic Acid (CH_3COOH). *Chem. Phys. Lett.* **2003**, *378*, 250–256. https://doi.org/10.1016/S0009-2614(03)01285-5.

(46) Sekiguchi, O.; Uggerud, E. Fragmentation of Deprotonated Glycolaldehyde in the Gas Phase and Relevance to the Formose Reaction. *J. Phys. Chem. A* **2013**, *117*, 11293–11296. https://doi.org/10.1021/jp4053715.

TOC Graphic